Journal of *Marine Science and Engineering*

MDPI

Article

Coastal Vulnerability Assessment for Future Sea Level Rise and a Comparative Study of Two Pocket Beaches in Seasonal Scale, Ios Island, Cyclades, Greece

Apostolia Komi [1], Alexandros Petropoulos [1], Niki Evelpidou [1,*], Serafeim Poulos [1] and Vasilios Kapsimalis [2]

[1] Faculty of Geology and Geoenvironment, National and Kapodistrian University of Athens, Panepistimiopolis, 15784 Athens, Greece
[2] Institute of Oceanography, Hellenic Centre for Marine Research, 19013 Anavyssos, Greece
* Correspondence: evelpidou@geol.uoa.gr

Abstract: The coastal zone may be considered as the location where the marine and land environments interact dynamically and coexist with human societies. Globally, natural and human systems are being severely threatened by the sea level rise related to climate change. The outcome between the dynamic relationship of coastal environments and marine processes, and the future sea level rise as predicted by scientific reports, is the vulnerability of coastal areas such as sandy beaches, pocket beaches and low-lying coastal areas. The current research aims to assess the coastal vulnerability of Ios Island, Cyclades, Greece for the next 100 years and to identify areas that are comparatively more vulnerable to future sea level changes. Moreover, the seasonal changes concerning sedimentological and morphological characteristics of two pocket beaches of Ios Island, Mylopotas and Magganari, are also examined. From the application of the Coastal Vulnerability Index, 92.37% of the total length of the coastline of Ios Island is characterized by a very low vulnerability as it consists of rocky shores and cliffs, while sandy and pocket beaches are characterized by a very high vulnerability. From the fieldworks and data processing, the seasonal changes mainly concern the seabed's topography, the sediments' texture of the collected sand samples, the foreshore and backshore topography, as well as seasonal shoreline displacement, using the Digital Shoreline Analysis System tool (DSAS).

Keywords: Coastal Vulnerability Index; shoreline changes; sea level rise; coastal geomorphology; coastal slope

check for updates

Citation: Komi, A.; Petropoulos, A.; Evelpidou, N.; Poulos, S.; Kapsimalis, V. Coastal Vulnerability Assessment for Future Sea Level Rise and a Comparative Study of Two Pocket Beaches in Seasonal Scale, Ios Island, Cyclades, Greece. *J. Mar. Sci. Eng.* **2022**, *10*, 1673. https://doi.org/10.3390/jmse10111673

Academic Editor: Chung-yen Kuo

Received: 30 September 2022
Accepted: 2 November 2022
Published: 6 November 2022

Publisher's Note: MDPI stays neutral with regard to jurisdictional claims in published maps and institutional affiliations.

Copyright: © 2022 by the authors. Licensee MDPI, Basel, Switzerland. This article is an open access article distributed under the terms and conditions of the Creative Commons Attribution (CC BY) license (https://creativecommons.org/licenses/by/4.0/).

1. Introduction

The coastal zone is a natural system that is directly affected by the interaction between the lithosphere, the hydrosphere and the atmosphere and by the action of land, air and marine processes. In addition to its unique natural features, the coastal zone is also of great interest for the abundance of resources it offers. About 41% of Europe's population lives near the coast, which leads to increasing rates of urbanization, as well as, the rapid development of the tourism industry [1]. Among the different types of coasts, sandy coasts bear the greatest burden from recreational activities [2] and are among the most geomorphologically complex coasts, with the coastline constantly changing under the interaction between natural and anthropogenic factors [3,4].

Coastal environments are in a dynamic relationship with marine processes where coastal sediments are constantly being moved, either resulting in the formation of a new coastline or the erosion of an existing coastline [5,6]. This dynamic interaction occurs over a wide range of time and space scales, leading to the evolution of the coastal zone. Temporal scales can range from seasonal to interannual changes, while space scales range from pocket beaches to open sea beaches [7–9]. The phenomenon of erosion is intensified by the rise of the sea level, as well as by anthropogenic interventions, thus increasing

the vulnerability of the coastal zones [10,11]. According to Vousdoukas et al., 2020 [3], 13.6–15.2% (36.097–40.511 km) of sandy coasts worldwide could experience severe erosion by 2050, increasing to 35.7–49.5% (95.061–131.745 km) by the end of the century.

In the case of Greece, the coastline reaches 18.400 km for the mainland country and 9.835 km for the island country [11]. Coastal erosion is estimated at 6.1% for Thrace and Eastern Macedonia, 10.3% for Central Macedonia, 2.3% for Thessaly, 14.7% for the North Aegean islands, 25.9% for the Cyclades and the Dodecanese, 3.8% for the Peloponnese and 6.1% for the coasts of Northern Crete [12]. In the Cyclades and Dodecanese region, 51% of the coastline consists of low slopes of 6–9% and 46% of pocket beaches with low slopes [12]. A pocket beach [13] is a small beach that is laterally bordered by two headlands. The headlands severely restrict any hydrosedimentary processes that might occur between their borders, turning them into an autonomous and independent environment. Pocket beaches have a more distinct circulation pattern than open sea beaches due to the hydrodynamic conditions and beach characteristics (slope, grain size, berm zones, etc.) [14].

Since the end of the 19th century, the global sea level has risen by about 1.6 mm/year [15], while its rate did not exceed 0.6 mm/year during the previous two millennia [16]. According to the report of the Intergovernmental Panel on Climate Change 2019 [17], the dominant sources of freshwater supply leading to a rise in the Global Mean Sea Level (GMSL) are glaciers and ice sheets. From tide gauge and satellite altimetry observations, GMSL has increased from 1.4 mm/yr during 1901–1990, to 2.1 mm/yr during 1970–2005, to 3.2 mm/yr during 1993–2015 and to 3.6 mm/year in the period 2006–2015. Estimations of future changes in this report are mainly based on the climate model CMIP by using Representative Concentration Pathways (RCPs). RCPs are scenarios that include the time series of emissions and concentrations of the full range of greenhouse gases (GHGs), aerosols and chemically active gases, as well as land use/land cover. At the end of the century, sea level rise is expected to be faster in all scenarios, including those compatible with reaching the long-term temperature target as defined by the Paris Agreement [18].

To assess coastal vulnerability to future sea level rise, various methods have been proposed and used from time to time, which are based on a number of parameters such as coastal geomorphology, the rate of sea level rise, the evolution of the coastline, etc., directly related to impending climate changes and how they will affect sea level. One of the most common methods is the Coastal Vulnerability Index (CVI) introduced by Gornitz et al., in 1991 [19]. It is a relatively simple and functional method which combines the sensitivity of the coastal zone to changes, with its ability to adapt to new conditions. By ranking the vulnerability of the coastal zone, it is feasible to identify the areas that are comparatively more vulnerable to sea level changes. The CVI was later modified [20] to include seven physical land/sea variables and six climate variables. The proposed, by Thieler and Hammer Klose (1999) [21], CVI is similar to that used by Gornitz et al. (1994) [20] and Shaw et al. (1998) [22]. This index allows six variables, three geological and three physical variables, to be linked in a quantifiable way. This method yields numerical data that cannot be directly equated with specific physical effects. However, it points to areas where the various impacts of sea level rise may be greatest [23–26]. Geological variables are geomorphology, shoreline displacement rate and coastal slope. They represent the shoreline's relative resistance to erosion, its long-term erosion/advance trend, and its vulnerability to flooding, respectively [27,28]. Physical process variables include significant wave height, tidal range and sea level change, which are related to the inundation risk of a particular stretch of shoreline on time scales of hours to centuries [27]. The method of the Coastal Vulnerability Index has already been applied in various case studies in Greece such as the Hellenic Aegean coast [29], Argolikos Gulf, Peloponnese [30] and the Gulf of Patras in Western Greece [31], as well as the Marathon beach in East Attica [32]. At international level, CVI has been applied on the U.S. Atlantic Coast [21], the Northern Coast of California [27], as well as in the eastern Mediterranean [33].

Taking into consideration the abovementioned risks to which coastal zones are subjected, i.e., the phenomenon of coastal erosion, future sea level rise and shoreline changes

due to sediment transport, the current research aims to two objectives. For the assessment of the coastal vulnerability, regarding the future sea level rise by 2100, the Coastal Vulnerability Index was applied. The study area, for the application of the index, is the coastal zone of Ios Island, located in central Cyclades, Greece. To examine seasonal changes, concerning the sedimentological, geomorphological and topographical coastal evolution in a restricted spatial scale, two pocket beaches of Ios Island were selected, Mylopotas Beach and Magganari Beach. The study periods for the seasonal changes concern autumn and spring period of 2018. For the purposes of the above seasonal approach, topographic cross sections and measurements along the shoreline of each study area were conducted by using Differential Global Positioning System (DGPS) with a Global Navigation Satellite System receiver (GNSS) of high precision, for the subsequent calculation of the shoreline displacement rate. Sediment sampling was also necessary for the current research.

2. Geographical and Geological Setting

The island of Ios is located in the Southeast Aegean Sea and belongs to the prefecture of Cyclades. The area of the island is approximately 108 km^2, with a coastline of 110 km. It has an elongated shape with a NW-SE direction and an axis length of 18 km of the longitudinal axis (NW-SE) and 8.5 km of the transversal axis (ENE-WSW) approximately (Figure 1).

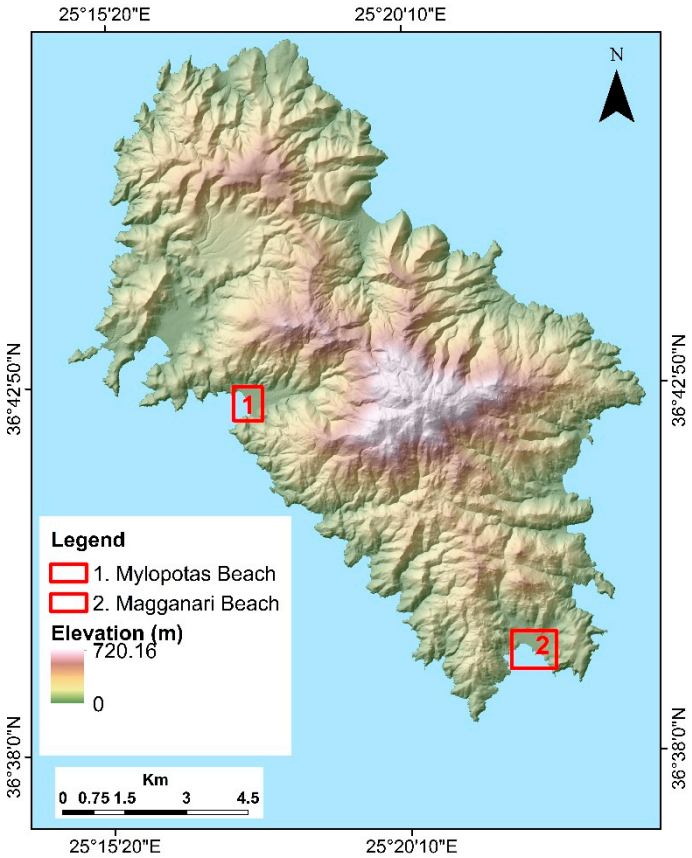


Figure 1. Location of study areas. In the west Mylopotas beach, while in the south is Magganari beach.

Ios is geologically divided into two main sections. The Cycladic basement and an overlying Blueschist unit mainly occur in the northern part of the island. The Quaternary formations occur as alluvial deposits in coastal plains and beaches with their components consisting mainly of fine-grained material [34].

Most of the rivers and streams of Ios originate from the mountainous part of the island and flow vertically towards the coastline. The largest branch of the hydrographic network

is of the 4th order according to Strahler, as produced by analyses of a Digital Elevation Model (DEM).

According to the climate data from the nearest meteorological station located in Naxos Island, 32 km NW from Ios Island, December records the highest amount of rain at 70.3 mm, while the lowest values are recorded during the summer months. The prevailing wind throughout the year is from the north and the maximum average monthly wind intensity occurs in the months of January and February [35].

According to the "Wind and Wave Atlas of the Greek Seas" [36], the wider area of Ios is characterized by an annual average significant wave height (Hs) of 0.7–0.8 m, annual average wind speed (Uw) 4–5 m/s and annual average wave period (Tp) 4.8–5.2 s.

From the CORINE 2018 database, it appears that the largest area of the island is covered by sclerophyllous vegetation (72.42%) and natural pastures (13.37%). The urban fabric covers only 1.1% of the island area and it is placed in the port and in Chora of Ios. The greatest development of tourist infrastructure is concentrated in Chora, the Port and Mylopotas beach, where most of the tourist accommodations (hotels, guesthouses, rooms for rent, etc.), catering facilities and recreational activities serving tourists are located [37].

2.1. Geographical Features of Mylopotas Beach

Mylopotas beach is located in western Ios with a total length of 700 m. It is bounded by two natural headlands and has a NW-SE direction. The upper limit of the beach is bounded by a low wall which separates it from the coastal road, beyond which the residential area extends. At the central part of the beach, the estuary of Mylopotas' stream is situated. The flow of the stream has been cut off by the construction of an upstream dam. Mylopotas beach is considered as the most touristic beach on Ios Island, gathering a variety of tourist businesses and leisure activities, the combination of which characterizes the beach with a strong anthropogenic impact (Figure 2).

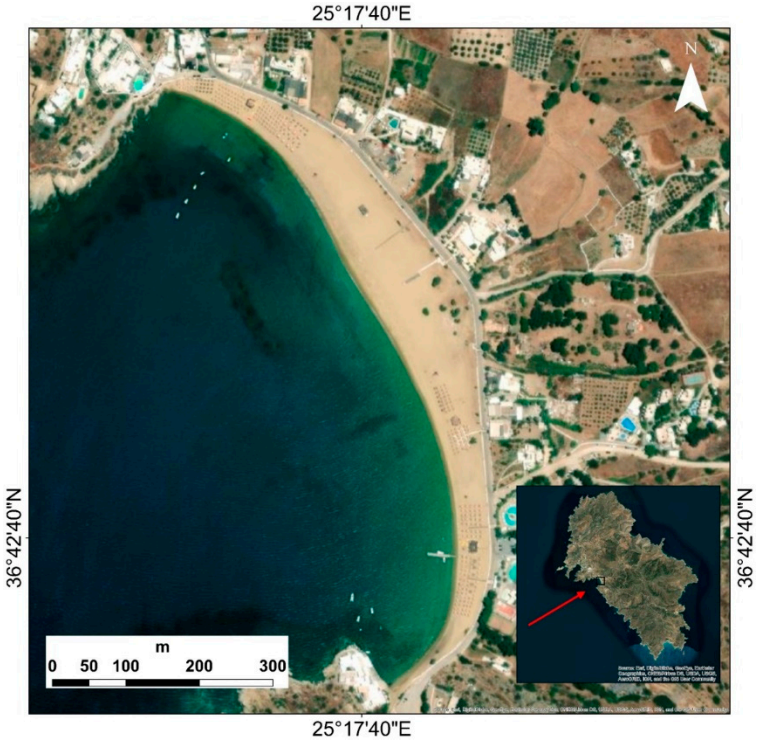


Figure 2. Mylopotas beach located in the western part of Ios. Red arrow indicates the position of the study area.

2.2. Geographical Features of Magganari Beach

Magganari beach is located at the southern end of Ios and consists of two bays running W-SE. The western bay is 343 m long, while the eastern bay is 300 m long. Unlike Mylopotas beach, Magganari does not host many tourist businesses, but it is a developing coastal area. The upper limit of the beach is bounded by sand dunes and vegetation (Figure 3).

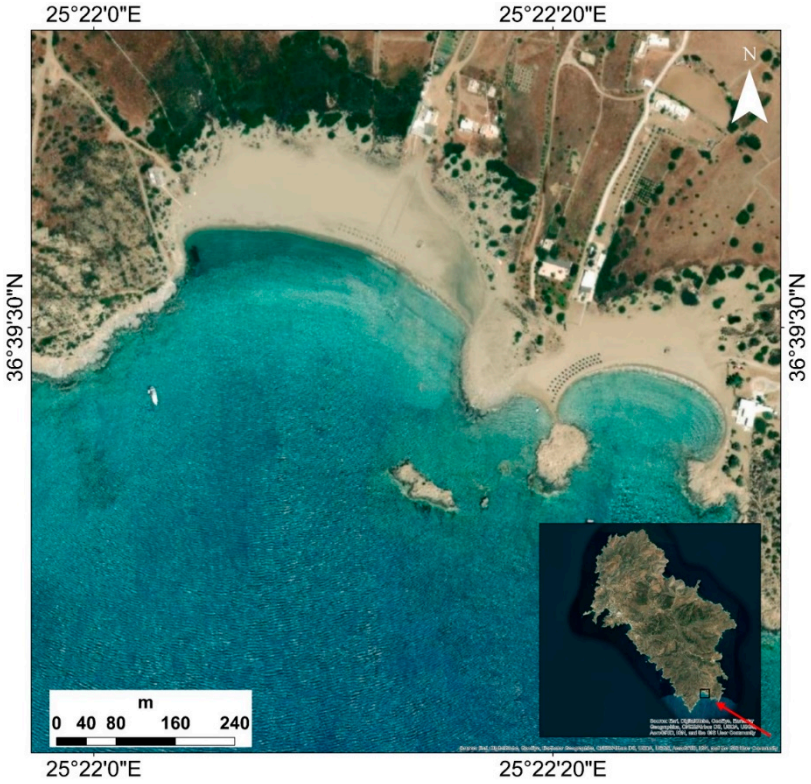


Figure 3. Magganari Beach is located at the southern part of Ios. Red arrow indicates the position of the study area.

3. Materials and Methods

3.1. Calculation of the Costal Vulnerability Index

Once the vulnerability value is determined for each section of coastline, based on the data for each variable, the CVI is calculated as the square root of the geometric mean, or the square root of the ranked variables divided by the total number of variables:

$$CVI = \sqrt{((a*b*c*d*e*f)/6)} \quad (1)$$

where: a = geomorphology, b = coastal slope, c = relative sea level change, d = shoreline displacement rate, e = mean tidal range and f = mean wave height.

We obtained the necessary data for each variable from orthophotos and topographical maps at a scale of 1:5000 from the Hellenic Military Geographical Service, and literature research. The Greek Geodetic Reference System 1987 (EGSA 87-GreekGrid) was chosen for the processing of the data and their mapping in the ArcGIS 10.3 environment.

For each variable, the coast was categorized into five vulnerability categories, (1) very low to (5) very high. Coast ranking ranges in the five vulnerability categories have been proposed by Pendelon et al. (2005) [27]. For the coastal slope variable, the ranges proposed by Alexandrakis et al., (2010) [12] were used (Table 1).

Table 1. Categorization of CVI variables according to Pendleton et al. (2004). A positive sign indicates shoreline advance, while a negative sign indicates retreat. For the coastal slope variable, the ranges proposed by Alexandrakis et al., (2010).

Variables/Ranking	Very Low 1	Low 2	Moderate 3	High 4	Very High 5
Geomorphology	Rocky-cliffed coasts, Fjords	Medium cliffs, Indented coasts	Low cliffs, Glacial drift, Alluvial plains	Cobble Beaches, Estuary, Lagoon	Barrier beaches, Sand beaches, Salt marsh, Mud flats, Deltas, Mangrove, Coral reefs
Coastal Slope (%)	>12	12–9	9–6	6–3	<3
Relative Sea Level Change (mm/yr)	<1.80	1.80–2.50	2.50–3	3–3.40	>3.40
Shoreline displacement rate (Erosion/Accretion) (m/yr)	>2	1–2	−1–+1	−1.10–−2	<−2
Mean Tidal Range (m)	>6.	4–6	2–4	1–2	<1
Mean Wave Height (m)	<0.55	0.55–0.85	0.85–1.05	1.05–1.25	>1.25

CVI Variables and Data

To assess the coastal geomorphology, medium and low-slope cliffs, rocky coasts, sandy beaches, estuaries and man-made structures were digitized in the ESRI ArcGIS 10.3 software environment. A 1:5000 topographic map of 4 m intervals from the Hellenic Military Geographical Service was used, in combination with orthophotos of the National Cadastre of the year 2010.

To calculate the coastal slope (in percent) of the study area, a Digital Elevation Model (DEM) was created using detailed contours of 4 m interval from 1:5000 topographic maps from the Army Geographical Service. In the ArcGIS 10.3 environment, the slope of the coastal zone from the coastline to the 6 m contour was calculated.

Two sea level change scenarios were applied to assess the coastal risk of Ios Island for the next 100 years. Specifically, according to the recent 2019 IPCC report, the RCP 2.6 scenario represents a low greenhouse gas emissions and high mitigation future. This scenario predicts a rise in GMSL over the next 100 years to 0.43 m at a rate of 4.3 mm/year. In contrast, the RCP 8.5 scenario represents high greenhouse gas emissions and a lack of policy to combat climate change, leading to a continued increase in atmospheric concentrations of greenhouse gases. This scenario predicts a rise in GMSL over the next 100 years to 0.84 m at a rate of 8.4 mm/year.

To determine the displacement rate of the coastline of Ios, orthophotos from the National Cadastre were used for the time periods of 2010 and 1996. The digitization of the two coastlines was carried out in the ArcGIS 10.3 environment and the calculation of the displacement rate of the coastline was carried out with the ArcGIS tool, DSAS 4.3 [38]. The statistical method used was End Point Rate (EPR). This method represents the distance of shorelines by the time elapsed between the oldest and the most recent shoreline

Taking into account the available Hydrographic Service statistics from a tide gauge in Syros Island, Cyclades, the average tidal range is 14 cm [39].

The wave heights that appear in the area, according to the Atlas of Winds and Waves of the Greek Seas [36] of the Hellenic Marine Research Center, are 0.7–0.8 m.

3.2. Fieldwork Investigation

The fieldwork investigation occurred at the two selected pocket beaches, Mylopotas and Magganari, in order to examine seasonal changes of their sedimentological, geomorphological and topographical features. The fieldwork investigation concerning the spring

profile of the study areas was carried out in April, while the fieldwork for the autumn profile was carried out in September of 2018.

3.2.1. Topographic-Geomorphological Mapping of Study Beaches

The on-site topographic-geomorphological mapping was carried out using a DGPS–GNSS. The mapping included measurements to delineate the landward upper limit of each beach, which often coincides with the growth of vegetation and/or the existence of man-made interventions (walls, road), as well as measurements along the current position of the coastline so that it is possible to compare the seasonal displacement of its position, if it exists. Additionally, during the fieldwork, we performed vertical topographic cross-sections. Specifically, altitude and depth measurements were carried out in relation to the coastline in order to capture the altitude differences and the width of the beaches. During the fieldwork that took place on Mylopotas beach, 41 topographical sections were made in April and 40 in September (Figure 4). During the fieldwork that took place at Magganari beach, 36 topographic sections were made in April and 42 in September (Figure 5).

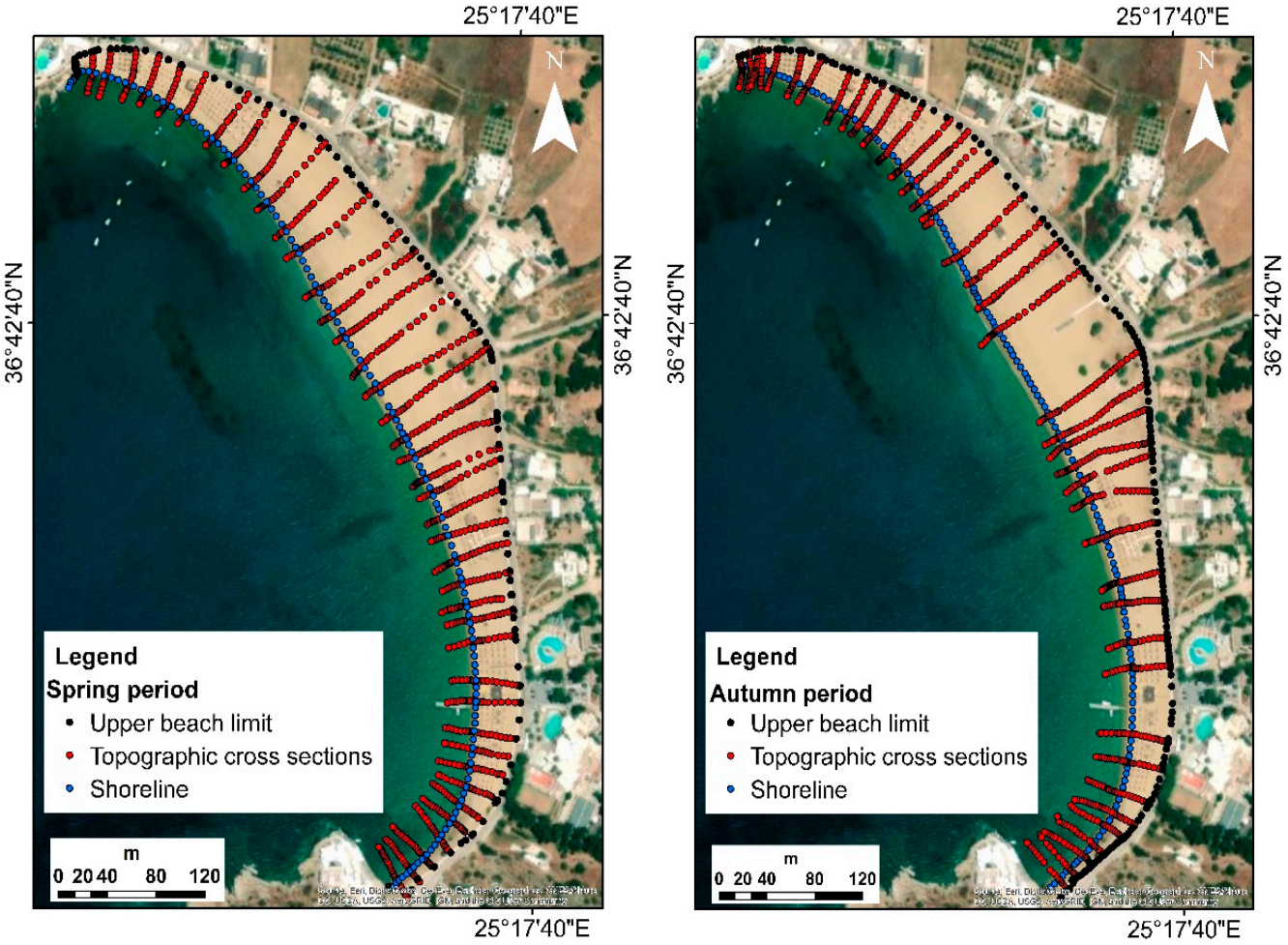


Figure 4. Mylopotas beach map. All dots are indicating DGPS measurement points: black dots indicate the inland beach limit, red dots indicate vertical cross sections in relation to shoreline, blue dots indicating the coastline during fieldwork period. (**a**) Spring profile fieldwork measurements (41 cross-sections). (**b**) Autumn profile fieldwork measurements (40 cross-sections) profile.

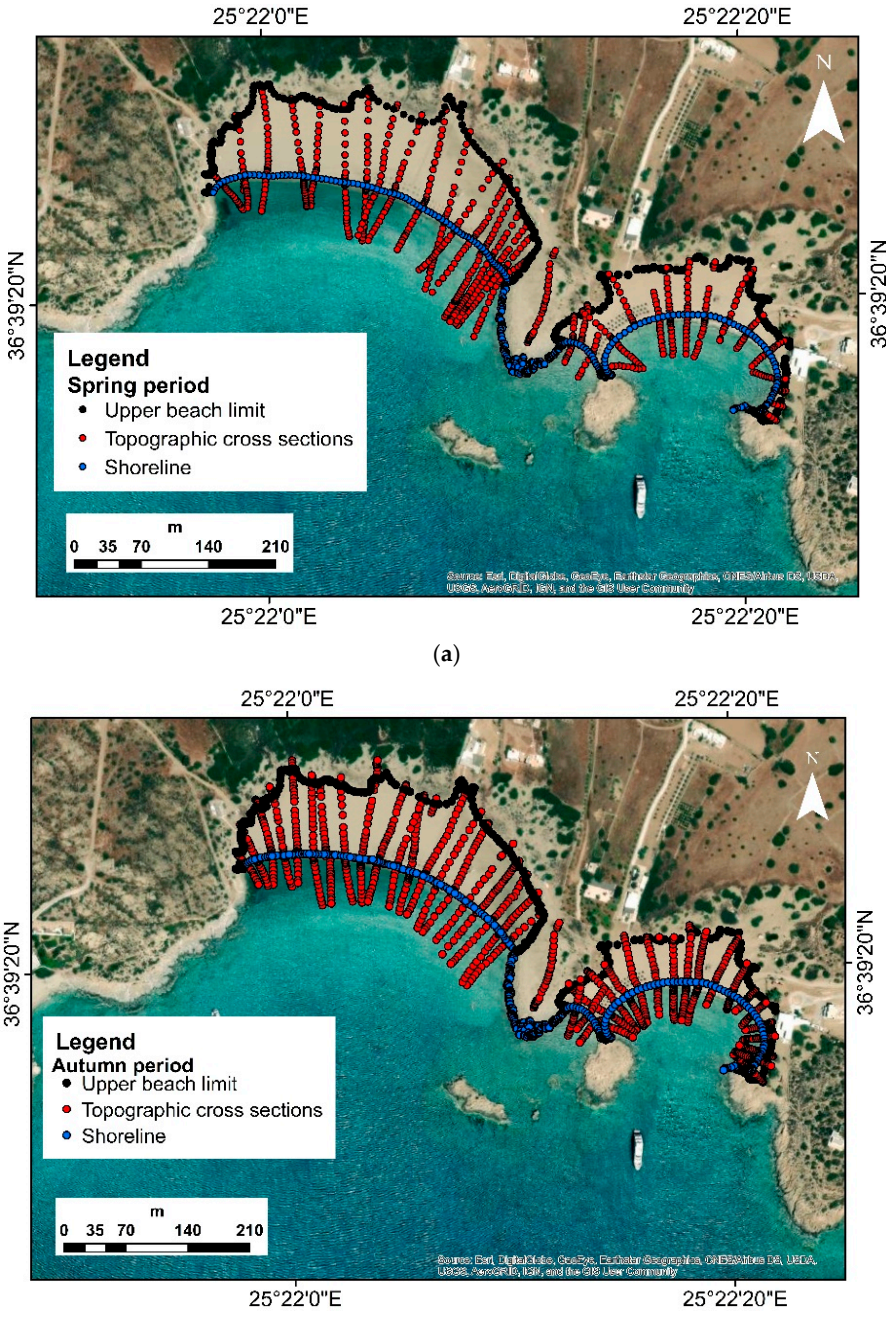


Figure 5. Magganari beach map. All dots are indicating DGPS measurement points: black dots indicate the inland beach limit, red dots indicate vertical cross sections in relation to shoreline, blue dots indicating the coastline during fieldwork period. (**a**) Spring profile fieldwork measurements (36 cross-sections). (**b**) Autumn profile fieldwork measurements (42 cross-sections) profile.

3.2.2. Sediments Sampling

During the implementation of the topographic measurements on the study beaches, it was deemed necessary to sample representative sediments in individual locations for the subsequent characterization of the material of each beach and to draw conclusions about the mean that transported the specific sediments and the depositional environment. The sampling sites represent points where changes in the composition of the beach material are observed.

For the synthesis of the spring profile of the beaches, 18 samples were collected from Mylopotas and 28 samples from Magganari. For the composition of the autumn profile, 19 samples were collected from Mylopotas and 30 from Magganari.

3.3. Laboratory Analyses

The laboratory analyses include the grain size analysis, using the dry sieving method for the sand samples collected from the study beaches, in order to determine the lithological character, grain size, grain size statistical parameters, grain size distribution and depositional mechanism. Sieves with diameters of 63 μm, 125 μm, 250 μm, 500 μm, 1 mm, 2 mm and 4 mm were used. In cases of coarser material than the sand-gravel boundary, 8 mm and 16 mm diameter sieves were also used. The finest material that passes through the sieve with the smallest diameter of 63 μm, is concentrated at the base of the sieve column and constitutes the silt-sand boundary. After the initial weight of each sample is noted, it is placed on the upper sieve and the column of sieves is transferred to the vibrating machine which is operated for 20 min at a power of 6 Hz. The statistical processing of the data resulting from the sieving was carried out using the program GRADISTAT v.4. The most important statistical parameters concern the mean size, sorting, skewness and kurtosis [40].

3.4. Calculation of Shoreline Displacement Rate

To calculate the seasonal changes of the shoreline at Mylopotas and Magganari, the measurements along the shoreline position from the fieldwork that took place in April and September 2018 were used. These measurements included the tide and atmospheric pressure for the given time periods. Because the tide values vary between 0.02–0.06 m, they do not bring about significant changes in the position of the coastline measured by the DGPS-GNSS. For the above calculations, the ArcGIS tool, DSAS 4.3, was used [38]. The statistical method used within the DSAS 4.3 tool was Net Shoreline Movement (NSM). This method refers to the total distance between the oldest and newest shorelines.

4. Results

4.1. CVI Results

Coastal Geomorphology

The main coastal landforms of the study area are medium and low cliffs, rocky coasts, steep cliffs, sandy beaches, estuaries and pocket beaches. This category also includes man-made structures, such as the port of Ios in the west and smaller boat marinas, which are characterized by very low vulnerability. Most of the coastal zone of Ios (93.29%) consists of rocky coasts and steep slopes and is characterized by very low vulnerability (Table 2). Sandy coasts and pocket beaches (5.13%) are characterized by very high vulnerability (Figure 6a).

Table 2. Ranking of the geological variables: Coastal Geomorphology; Coastal Slope; Shoreline displacement rate (Erosion/Accretion). The tables indicate the length, in km and percentage, of coastline in each category of vulnerability.

Vulnerability Ranking	Very Low (1)	Low (2)	Moderate (3)	High (4)	Very High (5)	Total
Coastal Geomorphology	Rocky, cliffed coasts Artificial constructions	Medium Cliffs	Low Cliffs	Cobble, pebble beaches Estuary	Sandy beaches, sandy pocket beaches	
Length (%)	93.29	0.24	0.18	1.16	5.13	100
Length (km)	102.77	0.27	0.20	1.27	5.65	110.10
Coastal Slope (%)	>12	12–9	9–6	6–3	<3	
Length (%)	95.07	1.36	1.47	0.92	1.18	100
Length (km)	104.74	1.50	1.61	0.92	1.30	110.10
Erosion/Accretion rate (m/yr)	>2	1–2	−1–1	−2–−1	<−2	
Length (%)			100			100
Length (km)			110.10			110.10

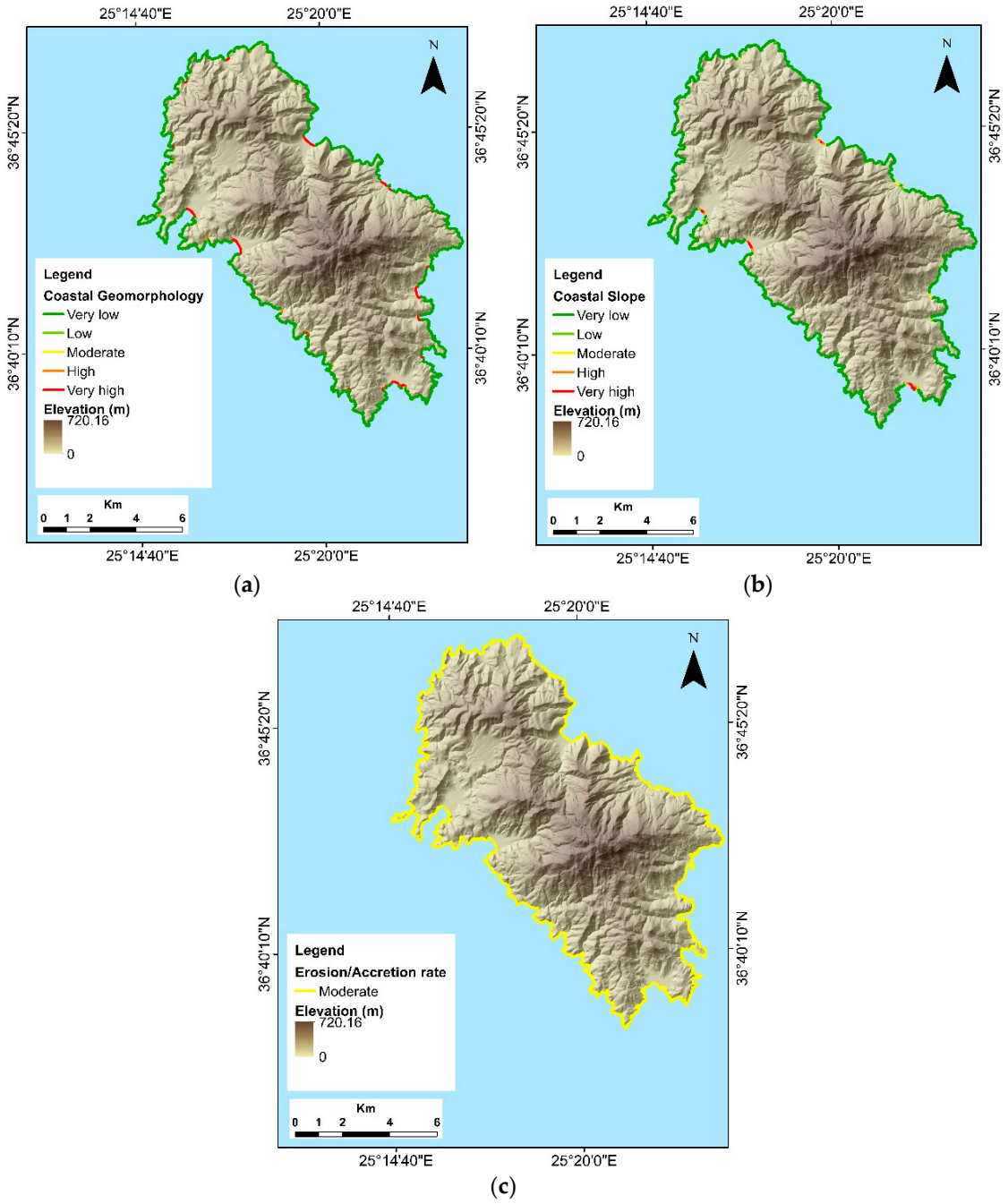


Figure 6. Map of vulnerability ranking of the geological variables: (**a**) Coastal Geomorphology; (**b**) Coastal Slope; (**c**) Shoreline displacement rate (Erosion/Accretion).

Coastal Slope

A total of 95.07% of the total length of the coastline is characterized by steep slopes of more than 12% and is, therefore, characterized by very low vulnerability (Table 2). As can be seen from the map, slopes below 3% are characterized by high vulnerability and are mainly represented by beaches and estuaries (Figure 6b).

Shoreline displacement rate

From the calculation of the displacement rate by using the DSAS tool, it appears that most of the coastline is characterized by a rate of −0.1–0.13 m/yr, while the displacement rate range is between −0.97–0.6 m/yr (Figure S1). For the calibration of the vulnerability, the ranges proposed in the literature are considered. Therefore, the displacement rate for

the entire coastline of Ios is included in the category of medium vulnerability, (Table 2 and Figure 6c).

Relative Sea Level change

The two IPCC 2019, scenarios, RCP 2.6 και RCP 8.5, for future sea level rise are characterized by very high vulnerability (Figure 7a and Table 3).

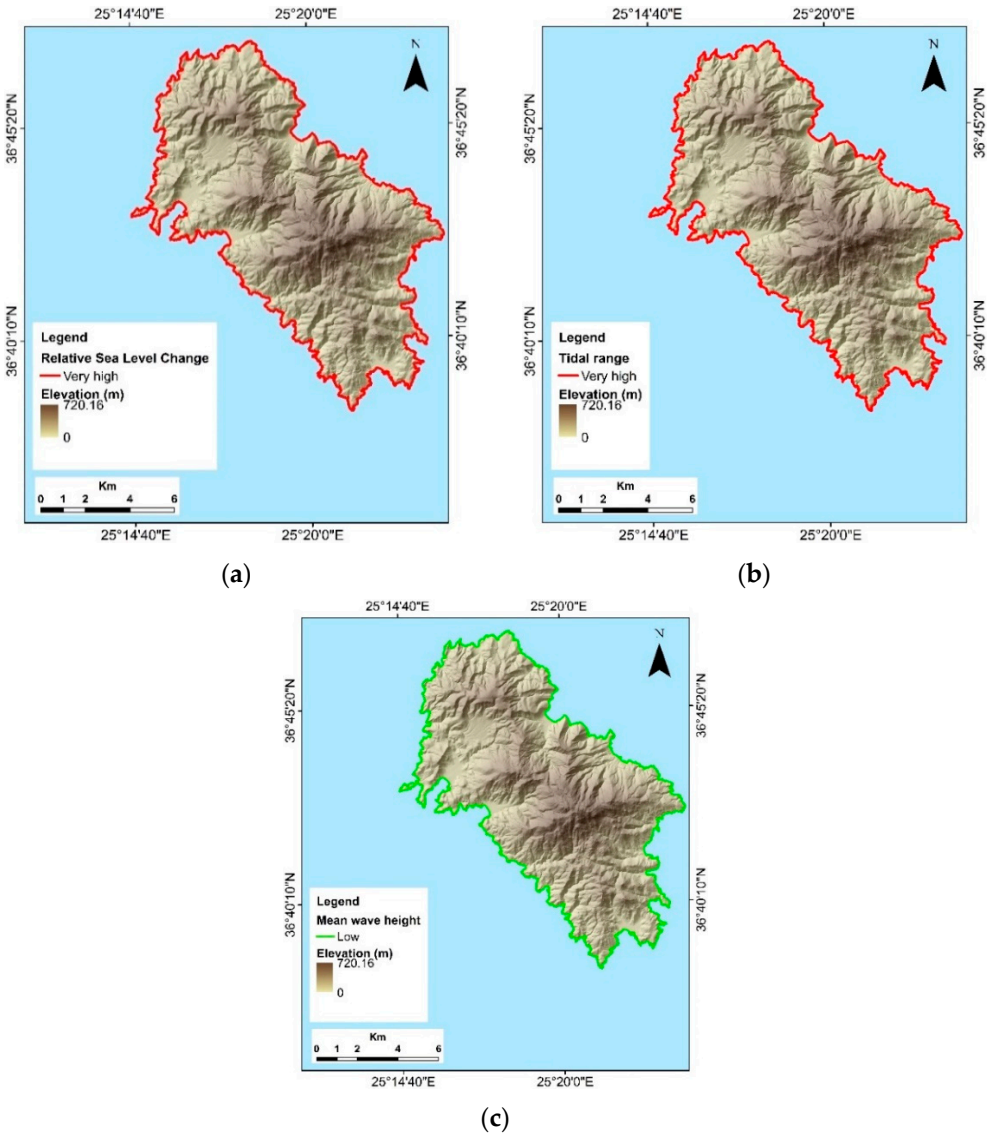


Figure 7. Map of vulnerability ranking of the physical variables: (**a**) Relative Sea Level change; (**b**) Tidal range; (**c**) Mean Wave Height.

Table 3. Ranking of the physical variables: (a) Relative Sea Level change; (b) Tidal range; (c) Mean Wave Height. The tables indicate the length, in km and percentage, of coastline in each category of vulnerability.

Vulnerability Ranking	Very Low (1)	Low (2)	Moderate (3)	High (4)	Very High (5)	Total
Relative sea level change (mm/yr)	<1.80	1.80–2.50	2.50–3	3–3.40	>3.40	
Length (%)					100	100
Length (km)					110.10	110.10
Tidal range (m)	>6	4–6	2–4	1– 2	<1	
Length (%)					100	100
Length (km)					110.10	110.10
Mean Wave Height (m)	<0.55	0.55–0.85	0.85–1.05	1.05–1.25	>1.25	
Length (%)		100				100
Length (km)		110.10				110.10

Tidal range

Taking into account the available data of the Hydrographic Service for the Cyclades, the average tidal range is 14 cm and was assumed to be the same along the entire coastline. Therefore, the entire coastline of Ios is included in the category of very high vulnerability (Figure 7b and Table 3).

Mean Wave Height

The mean annual significant wave height that appears in the area, is 0.7–0.8 m. Therefore, the entire coastline of Ios falls into the category of low vulnerability (Figure 7c and Table 3).

The CVI values

After the ranking of each variable, the mathematical calculation of the CVI was followed. The calculated CVI values along the coastline of Ios range from 5 to 25 (Table 4 and Figure 8).

Table 4. Ranking of the CVI values. The table indicates the length, in km and percentage, of coastline in each category of vulnerability.

Vulnerability Ranking	Very Low (1)	Low (2)	Moderate (3)	High (4)	Very High (5)	Total
CVI	5–7.07	7.07–10	10–11.18	11.18–19.36	19.36–25	
Length (%)	92.37	1.69	2.64	1.74	1.56	100
Length (km)	101.74	1.86	2.91	1.91	1.72	110.10

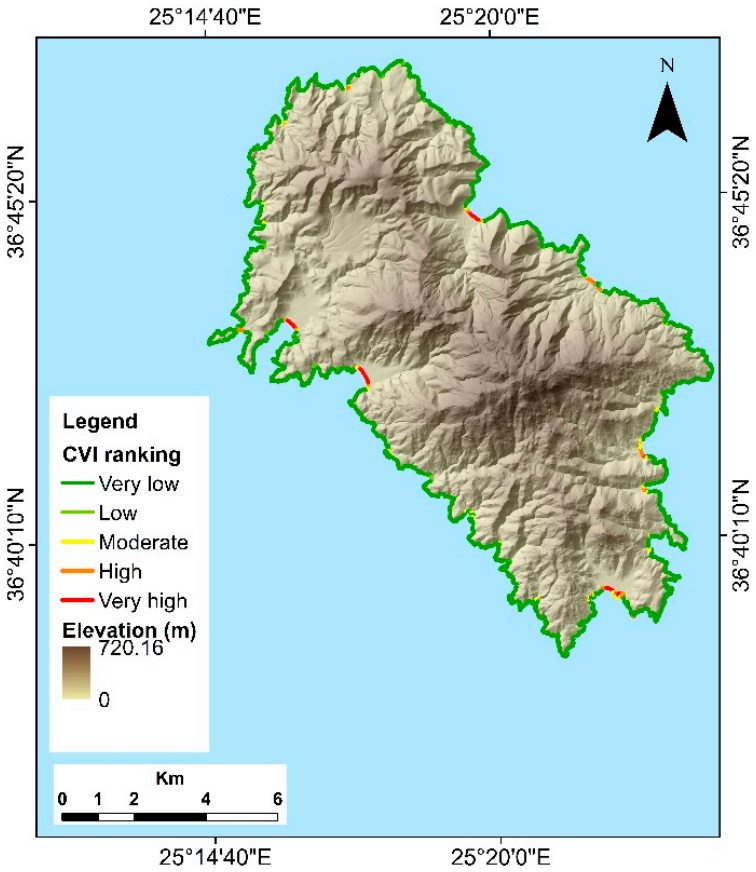


Figure 8. Map of vulnerability ranking of the CVI values.

4.2. Geomorphological Characteristics of Mylopotas and Magganari Beach

The detailed topographic mapping of Mylopotas and Magganari resulted in the presentation of their geomorphological seasonal characteristics through DEMs concerning the elevation and the slope of each beach at a seasonal scale.

At Mylopotas beach, the elevation indicates an accumulation of sediments mostly at the NW part of the beach for both seasons (Figure 9). According to the map of morphological slopes, the berm zone is identified along the coastline and preserved from April to September, with slope ranges between 12°–20° (Figure 10).

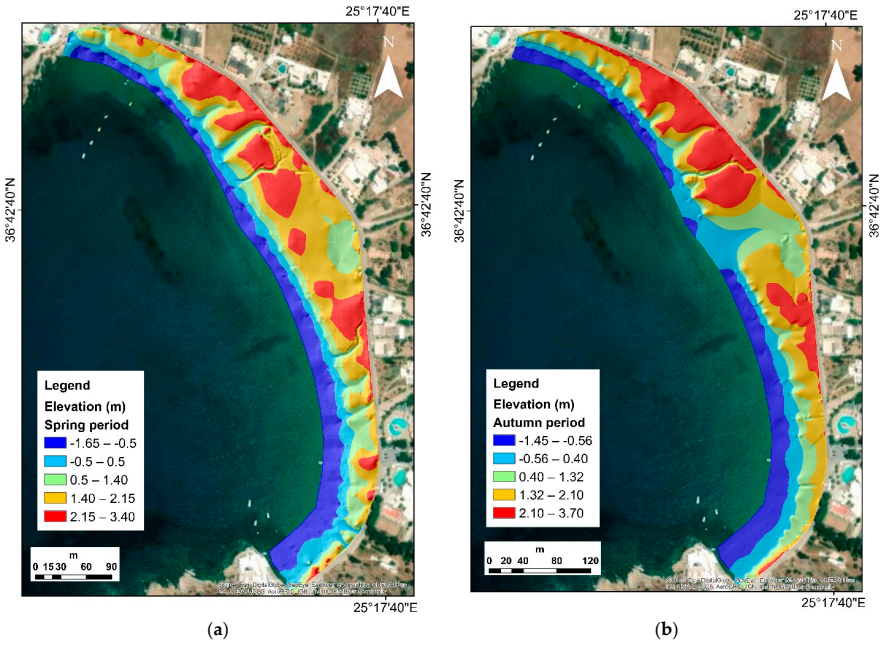


Figure 9. DEM of Mylopotas beach. (**a**) Shows the values of elevation from seaward to landward for the autumn period. (**b**) Shows the values of elevation from seaward to landward for the spring period.

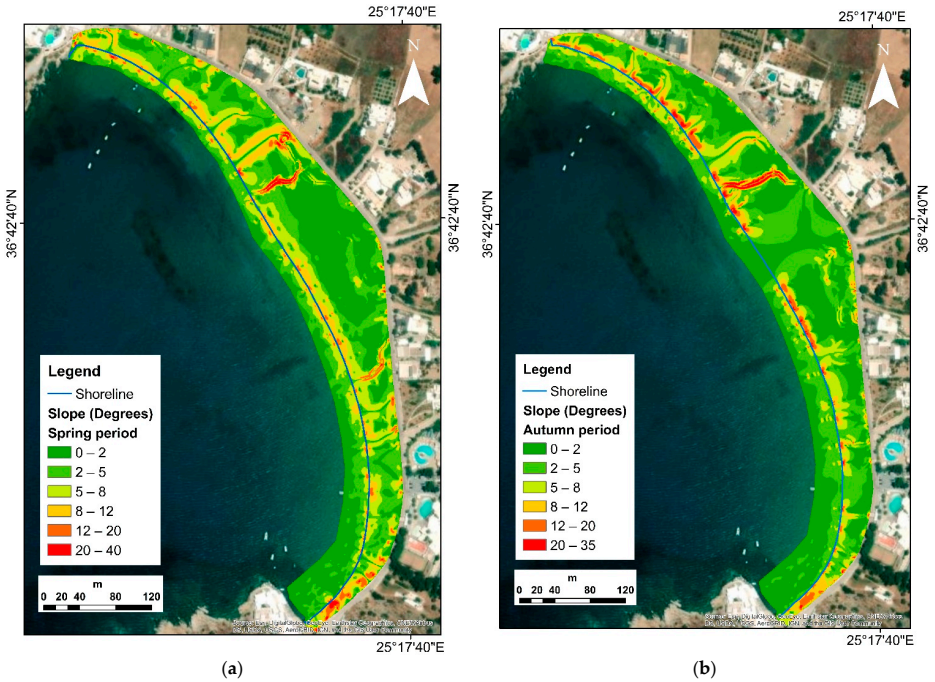


Figure 10. Map of morphological slopes of Mylopotas beach. (**a**) Shows the slope values from seaward to landward for the autumn period. (**b**) Shows the slope values from seaward to landward for the spring period. The left figure shows the slope values from seaward to landward for the autumn period.

At Magganari beach, the elevations at the landward part of the beach mostly ranged between 0.40–1.20 m for both seasons (Figure 11). According to the map of morphological

slopes, gentle slopes prevailed at most of the beach. The berm zone is identified along the coastline and preserved from April to September, with slope ranges between 10°–22°, with a maximum value of 25° during the autumn period (Figure 12).

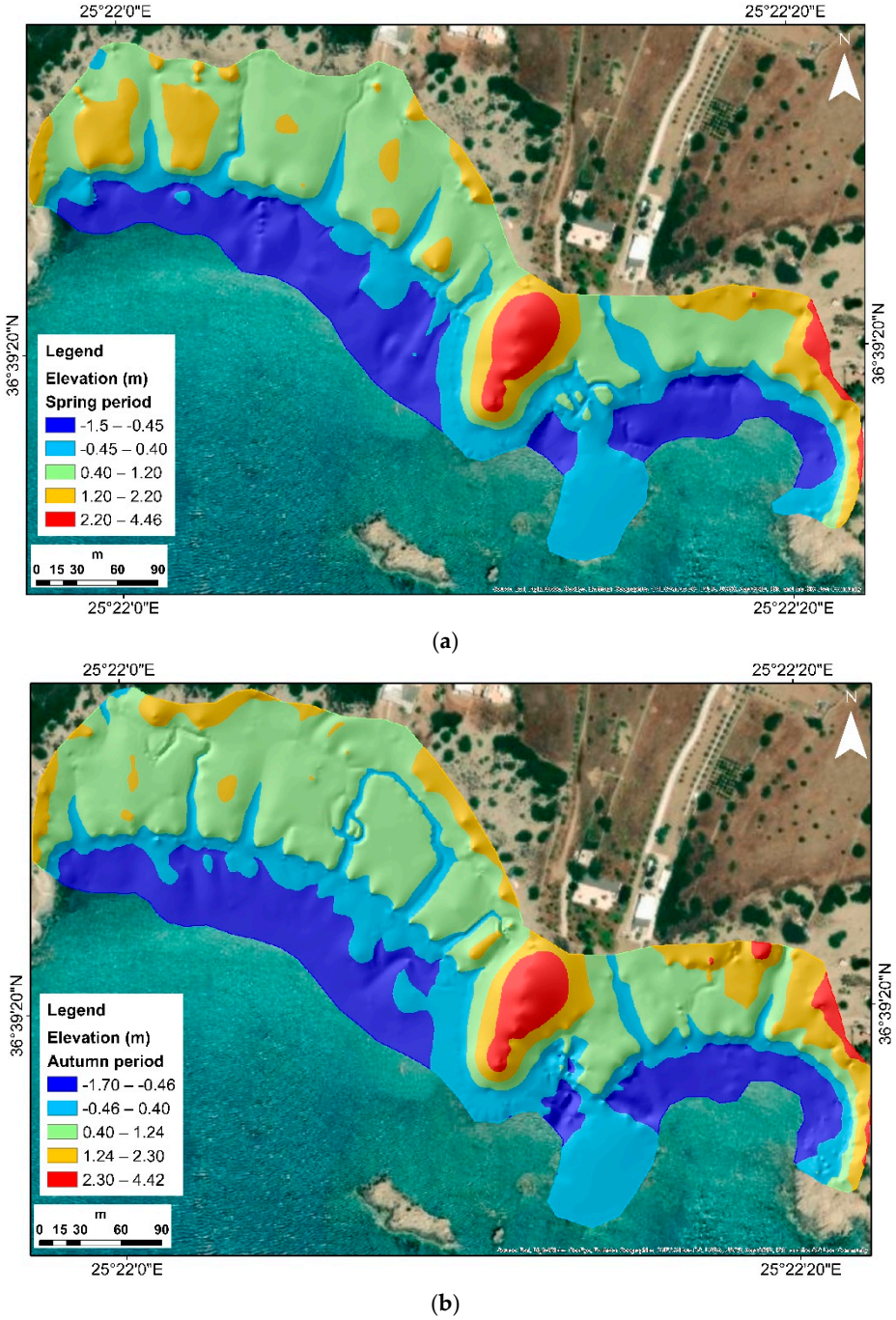
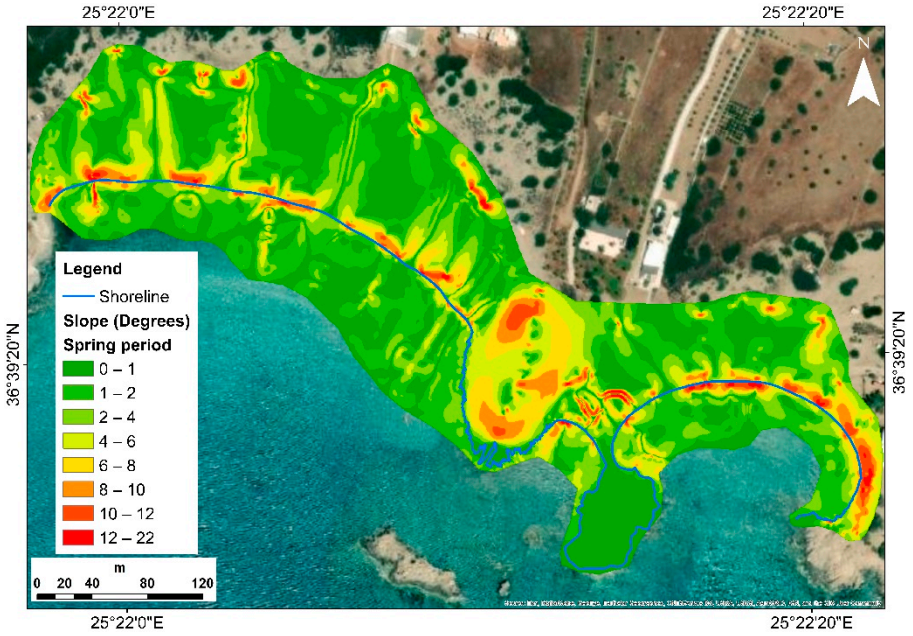
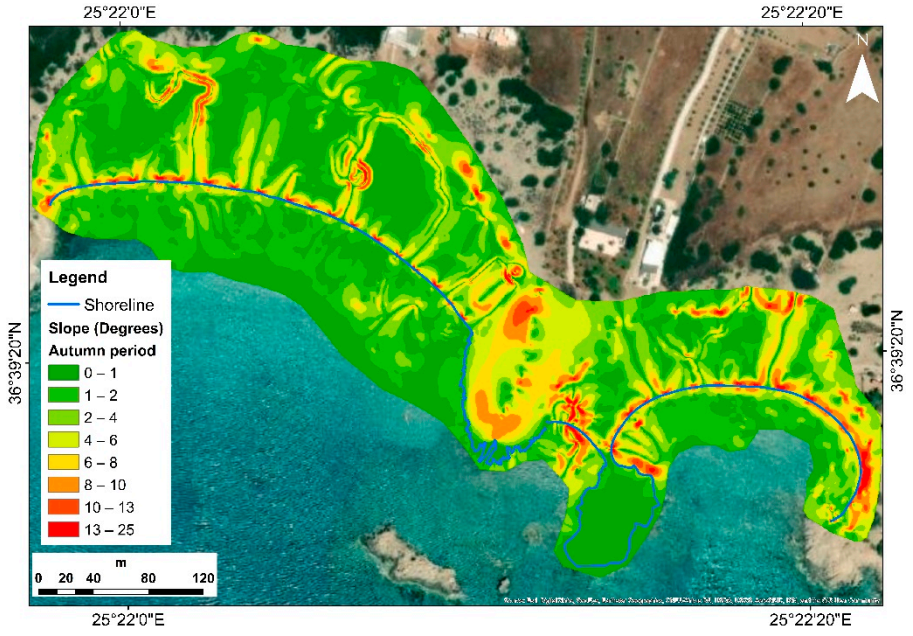


Figure 11. DEM of Magganari beach. (**a**) Shows the values of elevation from seaward to landward for the autumn period. (**b**) Shows the values of elevation from seaward to landward for the spring period.



(**a**)

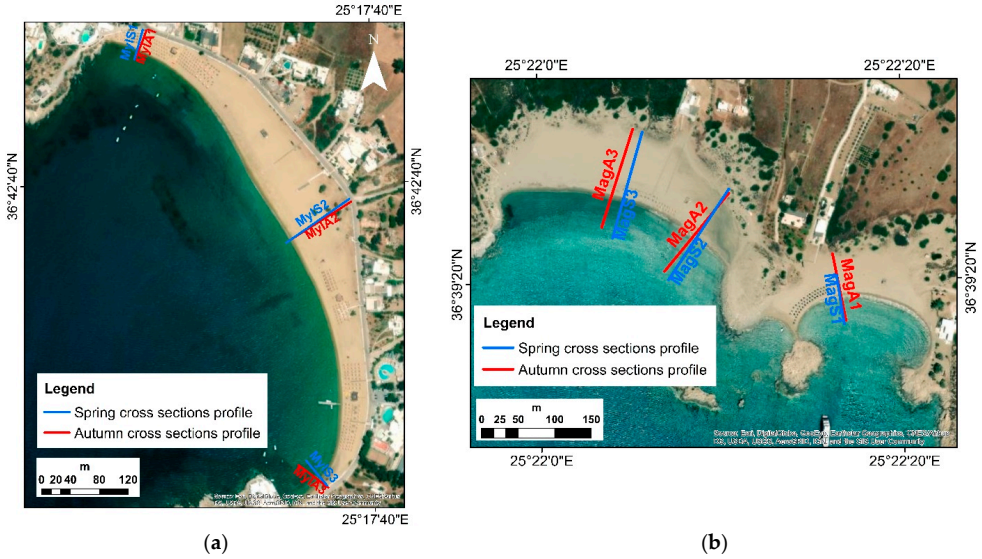


(**b**)

Figure 12. Map of morphological slopes of Magganari beach. (**a**) Shows the slope values from seaward to landward for the autumn period. (**b**) Shows the slope values from seaward to landward for the spring period.

4.3. Topographic and Sedimentological Characteristics

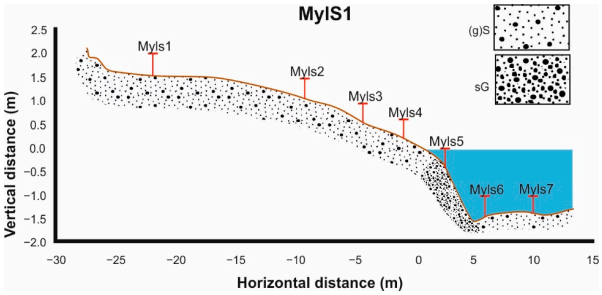
The results of the cross-sections and the grain-size analysis are presented below. From the topographic cross-sections that were carried out along the entire length of the beaches (Figures 4 and 5), due to the homogeneity of the topography, three positions were chosen from each beach which coincides for each study period, in order to be graphically illustrated. These positions are mainly located at the ends and the central part of each beach depending on its morphology (Figure 13).



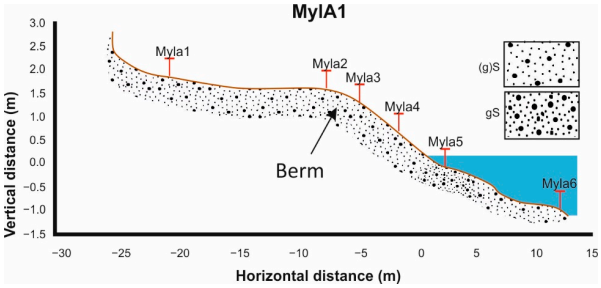
(**a**) (**b**)

Figure 13. Cross-sections of Mylopotas and Magganari: (**a**) For Mylopotas, cross-sections MylS1, MylS2 and MylS3 for the spring study period and cross-sections MylA1, MylA2 and MylA3 for the autumn study period; (**b**) For Magganari, cross-sections MagS1, MagS2 and MagS3 for the spring study period and cross-sections MagA1, MagA2 and MagA3 for the autumn study period.

In more detail, at the NW part of Mylopotas beach, the cross-section MylS1 presents a gentle slope, which at a distance of 5 m from the shoreline, becomes steep with the appearance of a 1.56 m deep graben. The MylA1 section is also characterized by a gentle slope and the distinct presence of a berm zone approximately 5 m landward from the coastline. The subsea section is characterized by a gentle slope. The prevailing beach material for both study periods is characterized by slightly gravelly sand, moderately sorted (Figure 14a,b).



(**a**)



(**b**)

Figure 14. Cross sections of the NW part of Mylopotas Beach: (**a**) Cross section MylS1 is represented by the samples Myls1, Myls2, Myls3, Myls4, Myls5, Myls6 and Myls7. Beach material is characterized by slightly gravelly sand (gS) and sandy gravel (sG). (**b**) Cross section MylA1 is represented by the samples Myla1, Myla2, Myla3, Myla4, Myla5 and Myla6. Beach material is characterized by slightly gravelly (g)S sand and gravely sand (gS). The arrow points to the berm zone along the cross-section.

In the central part of the beach, cross-sections MylS2 and MylA2 are characterized by stable topography on a seasonal scale. The first berm zone at a distance of 6.5 m from the coastline in MylS2 has been preserved in MylA2 and has been shifted to a distance of 7.5 m from the coastline. In the subsea section, the graben and subsequent ridge have been normalized. The beach material in MylS2 is characterized by alternations between slightly gravelly sand and gravelly sand, which turns into sandy gravel and gravelly sand underwater, mostly moderately sorted. At section MylA2 a continuous occurrence of slightly gravelly sand is noted, which grades into gravelly sand towards the shoreline, the majority of the samples are moderately sorted (Figure S2a,b).

In the southern part of the beach, the topography, as presented by cross-sections MylS3 και MylA3, does not differ for the two seasonal profiles. The material of the beach changes from sandy gravel to sand with the predominance of very platykurtic kurtosis and very fine skewness. Cross-section MylA3 is characterized by slightly gravelly sand, coarse skewed and mainly moderately sorted (Figure S3a,b).

Cross-sections MagS1 and MagA1 represent the eastern bay of Magganari beach, where the berm zone is observed. Toward the coastline, the slope becomes steeper, with a graben occurring approximately 6 m from the coastline for both profiles. The beach material of the eastern bay is characterized by the successive appearance of slightly gravelly sand and sand, during the spring profile, while during the autumn slightly gravelly sand prevails. The majority of the samples are moderately well sorted (Figure S4a,b).

Cross-sections MagS2 and MagA2 are located in the western bay of the beach. The upper limit of the beach is steep due to the presence of dunes, and then the slope is normalized. The berm zone is distinguished. Along MagA2, the subsea slope is gentle with the appearance of a mild ridge. Along MagS2, two successive grabens and ridges appear at a short distance from the coastline beyond which the slope becomes gentle. The sedimentological characteristics present a similar sedimentological regime to that of the eastern bay's sections (Figure S5a,b).

Cross-section MagS3 is characterized by a gentle slope until the appearance of a graben. From the berm zone to the coastline the slope becomes steeper. Along cross-section MagA3 two grabens appear at the land part of the beach. The beach material is characterized by slightly gravelly sand and a coarse skewness in both cross-sections, with the appearance of gravelly sand only in the spring profile (Figure S6a,b).

4.4. Seasonal Shoreline Displacement

In the northern part of the beach of Mylopotas, the spring coastline in relation to the autumn one undergoes a retreat of 4.9–3 m. Towards the central part, this retreat decreases and was estimated between −3 m and −2 m. The central part of the beach is characterized by a retreat between −2 m and −1 m, which towards the southern part increases between −3 m and −2 m. In the central part, there is a small advance of the autumn coastline compared to the spring coastline, which does not exceed 0.4 m. In the southern part, the retreat of the spring coastline in relation to the autumn coastline continues and ranges mainly between −2 m and −3.8 m. At the southern end of the beach, the displacement is almost zero (Figure 15).

At the eastern end of Magganari beach, the spring coastline is retreating in the range of 1.72–0.54 m compared to the autumn coastline. Toward the tombolo, the autumn shoreline advances in relation to the spring shoreline from 0.65 m to as much as 5 m. In the western part, the displacement of the coastline is almost zero, in some places, the advance of the autumn coastline is from 0.65 m up to 3.54 m. The advanced land that separates the east and the western bay and the tombolo do not present any seasonal displacement (Figure 16).

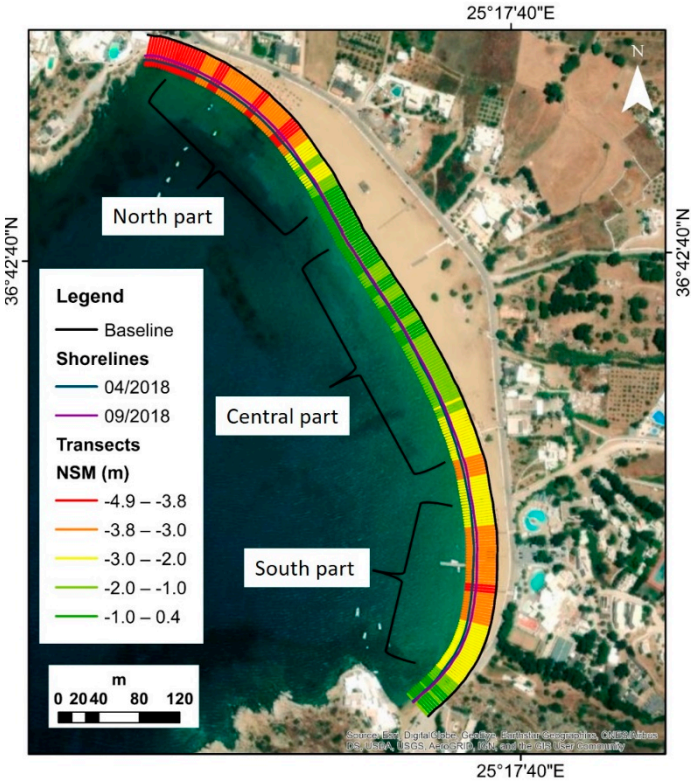


Figure 15. Map of seasonal displacement of the shoreline at Mylopotas beach.

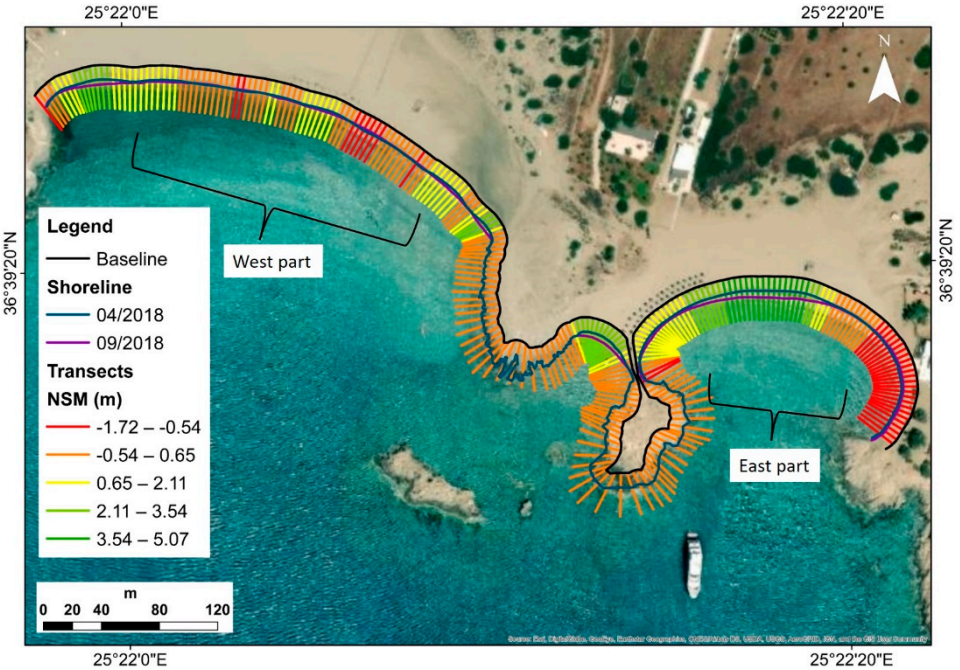


Figure 16. Map of seasonal displacement of the shoreline at Magganari beach.

5. Discussion

Examining the overall vulnerability of the coastal zone of Ios, to future sea level rise it is evident that among the five classification categories (Tables 2 and 3), the distribution of vulnerability is uneven with very low vulnerability predominating. Physical variables, as well as shoreline displacement from geologic variables, are represented by one ranking class each, for the entire length of the coastline. Therefore, the variables that mainly contribute

to CVI values are coastal geomorphology and coastal slope. Specifically, according to coastal geomorphology, 93.29% of the total length of the shoreline consists of rocky-cliffed coasts. The rocky coasts of Ios island consist of schists, gneisses and marbles, which are very resistant to erosion [34]. Regions with a coastal slope of more than 12% occupy 95.07% of the total length of the shoreline. Since low-sloping coastal zones should retreat more quickly than steeper regions, the determination of regional coastal slope indicates the relative vulnerability to inundation and the potential speed of the shoreline retreat [27]. Thus, for each of the above variables, almost the entire length of the shoreline is characterized by the low vulnerability. The parts of the coastline represented by sandy beaches or pocket beaches of fine-grained material and a low slope (<3%), are characterized by very high vulnerability and concern a minimal percentage (5.13% and 1.18%) of the total length of the coastline. These areas exhibit the greatest vulnerability to future sea level rise.

By comparing the seasonal cross-sections of Mylopotas beach, the north part of the beach is characterized by a gentle slope during the spring profile, while the autumn profile is characterized by the distinct presence of a berm zone. Moreover, the subsea section differs morphologically in seasonal scale, with the appearance of a steep graben along the spring cross-section and a gentle shallower relief along the autumn cross-section. The two profiles indicate mostly similar sedimentological characteristics, with the beach material mainly characterized as slightly gravelly sand. In the central part of the beach, the two profiles are characterized by almost similar topography on a seasonal scale. Of the two berm zones in the spring profile, one has been preserved in the autumn profile. In the subsea section, the relief has been normalized to the autumn profile. There are sedimentological variations between seasonal cross-sections with the predominance of slightly gravelly sand and gravelly sand. In the southern part of the beach, the topography does not differ for the two seasonal profiles. It is obvious that the berm zone from the central part of the beach to the south has been normalized. The slightly gravelly sand prevails in the autumn profile, while in the spring there are changes in the material of the beach.

By comparing the seasonal cross-sections of Magganari beach, the eastern bay is characterized by the distinct presence of the berm zone. Towards the coastline, the morphological characteristics are mostly similar for both profiles, with a steep slope and the occurrence of a graben and a subsequent ridge. In the autumn profile, the depth of the graben and the size of the ridge decrease. Sedimentologically, slightly gravelly sand and sand prevailed. The two seasonal profiles of the western bay also show similar topography mainly on the landward part of the beach with the occurrence of a steep upper limit, a gentle slope and a distinct berm zone. Differences are noted in the subsea section, where during the autumn study period, the slope of the bottom is normalized, while during the spring period, two successive grabens and ridges appear. Sedimentological is similar to that of the cross-sections of the eastern bay. In the subsequent profiles of the western bay, the berm zone has been preserved, as have the grabens at a short distance from it. Towards the coastline, the slope becomes steep in both profiles. From the spring to the autumn period the bottom becomes shallower and the autumn profile is characterized by the existence of a graben with a subsequent ridge. The material of the beach is characterized by the predominance of slightly gravelly sand.

At Mylopotas beach, the retreat of the coastline prevails, from the spring to the autumn study period, mainly in the northern and southern parts of the beach. This retreat is mainly between 3 and 4.9 m. Most of the coastline in the central part of the beach does not indicate a seasonal displacement, while at the points where the autumn coastline advances, it does not exceed 0.4 m. At Magganari Beach most of the coastline remains constant between the two seasons. The greatest displacement occurs in the eastern part, with the autumn coastline advancing compared to the spring coastline by up to 5 m towards the sea.

6. Conclusions

In this study, the coastal zone of Ios Island was studied in terms of coastal vulnerability in relation to future sea level rise, as well as the topographical–geomorphological and

sedimentological characteristics of two pocket beaches Mylopotas and Magganari, in relation to seasonal changes indicating their coastal evolution.

Coastal geomorphology, combined with coastal slopes, are the main geological parameters, under which most of the coastline of Ios (101.74 km) is characterized by very low vulnerability to future sea level rise by 2100. This condition is also confirmed by the calculation of the displacement rate of the coastline in the framework of the application of the CVI. In a period of 14 years (1996–2010), the displacement (advancement/erosion) that occurred on the coastline of Ios mostly concerns coastal areas with <3% slope, such as sandy beaches and pocket beaches, and is between −1–1 m/yr, in contrast to rocky-cliffed coasts where their displacement is almost zero.

At Mylopotas beach, slightly gravelly sand prevails, with the berm zone being more distinct during the autumn season. The observed normalization of the bottom from the spring to the autumn period is probably due to the action of summer waves which tend to smooth the topography of the sea bottom. A similar sedimentological regime prevails at Magganari beach. The majority of the sediments are characterized as slightly gravelly sand, while the presence of sand is greater than in Mylopotas. The berm zone has been maintained in both study periods. A shallowness of the bottom is observed with the preservation of the morphology in the eastern bay. At the western bay, bottom smoothing is observed in the autumn study period, with no material removed or added.

In the case of Mylopotas, the calculated retreat of the coastline is probably due to the reduced lateral supply of sediment as it is a pocket beach, enclosed by rocky formations, combined with intense tourist activity. The construction of the dam upstream of the Mylopotas stream has limited the supply of sediment to the beach. Part of the material removed from the northern part of the beach is possibly preserved within the break zone, justifying the shallowness observed in the northern part of the beach during the autumn profile. At Magganari, the limited tourist activity and the preservation of the natural landscape favors the supply of the beach through the hydrographic network and the retention of the sediment between the seasons. This condition is evident by the calculated advance of the coastline from the spring to the autumn study period, but also by the almost zero displacements of the coastline in most of the beach.

Supplementary Materials: The following supporting information can be downloaded at: https://www.mdpi.com/article/10.3390/jmse10111673/s1, Figure S1: Map of the calculated shoreline displacement rate between the years 1996 and 2010 using the DSAS tool; Figure S2: Cross sections of the central part of Mylopotas Beach; Figure S3: Cross sections of the southern part of Mylopotas Beach; Figure S4: Cross sections of the eastern bay of Magganari Beach; Figure S5: Cross sections of the western bay of Magganari Beach; Figure S6: Cross sections of the western bay of Magganari Beach.

Author Contributions: Conceptualization, A.K., A.P. and N.E.; methodology, A.K., A.P., N.E., S.P. and V.K.; software, A.K.; formal analysis, A.K.; investigation, A.K. and A.P.; resources, A.K. and A.P.; writing—original draft preparation, A.K.; writing—review and editing, A.K., A.P., N.E., S.P. and V.K.; visualization, A.K.; supervision, N.E. All authors have read and agreed to the published version of the manuscript.

Funding: This research received no external funding.

Institutional Review Board Statement: Not applicable.

Informed Consent Statement: Informed consent was obtained from all subjects involved in the study.

Data Availability Statement: Not applicable.

Acknowledgments: Authors would like to thank Giannis Saitis for editing in this paper.

Conflicts of Interest: The authors declare no conflict of interest.

References

1. Collet, I.; Engelbert, A. Coastal Regions: People Living along the Coastline, Integration of NUTS 2010 and Latest Population Grid. *EUROSTAT Stat. Focus* **2013**, *30*.
2. Davenport, J.; Davenport, J.L. The Impact of Tourism and Personal Leisure Transport on Coastal Environments: A Review. *Estuar. Coast. Shelf Sci.* **2006**, *67*, 280–292. [CrossRef]
3. Vousdoukas, M.I.; Ranasinghe, R.; Mentaschi, L.; Plomaritis, T.A.; Athanasiou, P.; Luijendijk, A.; Feyen, L. Sandy Coastlines under Threat of Erosion. *Nat. Clim. Chang.* **2020**, *10*, 260–263. [CrossRef]
4. Mentaschi, L.; Vousdoukas, M.I.; Pekel, J.-F.; Voukouvalas, E.; Feyen, L. Global Long-Term Observations of Coastal Erosion and Accretion. *Sci. Rep.* **2018**, *8*, 12876. [CrossRef]
5. Aiello, A.; Canora, F.; Pasquariello, G.; Spilotro, G. Shoreline Variations and Coastal Dynamics: A Space–Time Data Analysis of the Jonian Littoral, Italy. *Estuar. Coast. Shelf Sci.* **2013**, *129*, 124–135. [CrossRef]
6. Petropoulos, A.; Kapsimalis, V.; Evelpidou, N.; Karkani, A.; Giannikopoulou, K. Simulation of the Nearshore Sediment Transport Pattern and Beach Morphodynamics in the Semi-Enclosed Bay of Myrtos, Cephalonia Island, Ionian Sea. *J. Mar. Sci. Eng.* **2022**, *10*, 1015. [CrossRef]
7. Psomiadis, E.; Parcharidis, I.; Poulos, S.; Stamatis, G.; Migiros, G.; Pavlopoulos, A. Earth Observation Data in Seasonal and Long Term Coastline Changes Monitoring the Case of Sperchios River Delta (Central Greece). *Zeitschrift fur Geomorphol. Suppl.* **2005**, *137*, 159–175.
8. Ruggiero, P.; Kaminsky, G.M.; Gelfenbaum, G.; Voigt, B. Seasonal to Interannual Morphodynamics along a High-Energy Dissipative Littoral Cell. *J. Coast. Res.* **2005**, *21*, 553–578. [CrossRef]
9. Norcross, Z.M.; Fletcher, C.H.; Merrifield, M. Annual and Interannual Changes on a Reef-Fringed Pocket Beach: Kailua Bay, Hawaii. *Mar. Geol.* **2002**, *190*, 553–580. [CrossRef]
10. Bombino, G.; Barbaro, G.; D'Agostino, D.; Denisi, P.; Foti, G.; Labate, A.; Zimbone, S.M. Shoreline Change and Coastal Erosion: The Role of Check Dams. First Indications from a Case Study in Calabria, Southern Italy. *CATENA* **2022**, *217*, 106494. [CrossRef]
11. Poulos, S.E.; Chronis, G. The Importance of the River Systems in the Evolution of the Greek Coastline. In *CIESM Science Series*; CIESM: Cambados, Spain, 1997; pp. 75–96.
12. Alexandrakis, G.; Karditsa, A.; Poulos, S.; Ghionis, G.K.N.A. An Assessment of the Vulnerability to Erosion of the Coastal Zone Due to a Potential Rise of Sea Level: The Case of the Hellenic Aegean Coast. In *Environmental Systems –Volume III.*; Achim, S., Ed.; Eolss: Oxford, UK, 2010; p. 324.
13. Bowman, D.; Guillén, J.; López, L.; Pellegrino, V. Planview Geometry and Morphological Characteristics of Pocket Beaches on the Catalan Coast (Spain). *Geomorphology* **2009**, *108*, 191–199. [CrossRef]
14. Klein, A.H.F.; Ferreira, Ó.; Dias, J.M.A.; Tessler, M.G.; Silveira, L.F.; Benedet, L.; de Menezes, J.T.; de Abreu, J.G.N. Morphodynamics of Structurally Controlled Headland-Bay Beaches in Southeastern Brazil: A Review. *Coast. Eng.* **2010**, *57*, 98–111. [CrossRef]
15. Church, J.A.; White, N.J. Sea-Level Rise from the Late 19th to the Early 21st Century. *Surv. Geophys.* **2011**, *32*, 585–602. [CrossRef]
16. Kemp, A.C.; Horton, B.P.; Donnelly, J.P.; Mann, M.E.; Vermeer, M.; Rahmstorf, S. Climate Related Sea-Level Variations over the Past Two Millennia. *Proc. Natl. Acad. Sci. USA* **2011**, *108*, 11017–11022. [CrossRef] [PubMed]
17. Portner, H.O.; Roberts, D.C.; Masson-Delmotte, V.; Zhai, P.; Tignor, M.; Poloczanska, E.; Mintebeck, K.; Nicolai, M.; Okem, A.; Petzold, J.; et al. IPCC The Ocean and Cryosphere in a Changing Climate Summary for Policmakers. *IPCC Spec. Rep. Ocean Cryosph. a Chang. Clim.* **2019**, 42.
18. Oppenheimer, M.; Glavovic, B.C.; Hinkel, J.; van de Wal, R.; Magnan, A.K.; Abd-Elgawad, A.; Cai, R.; Cifuentes-Jara, M.; DeConto, R.M.; Ghosh, T.; et al. Sea Level Rise and Implications for Low-Lying Islands, Coasts and Communities. In *IPCC Special Report on the Ocean and Cryosphere in a Changing Climate*; The Intergovernmental Panel on Climate Change: Geneva, Switzerland, 2019.
19. Gornitz, V.; White, T.W.; Cushman, R.M. Vulnerability of the US to Future Sea Level Rise. In Proceedings of the Symposium on Coastal and Ocean Management, Long Beach, CA, USA, 8–12 July 1991.
20. Gornitz, V.M.; Daniels, R.C.; White, T.W.K.R. Birdwell The Development of a Coastal Vulnerability Assessment Database, Vulnerability to Sea-Level Rise in the U.S. Southeast. *J. Coast. Res.* **1994**, *12*, 327–338.
21. Thieler, E.R.; Hammar-Klose, E.S. *National Assessment of Coastal Vulnerability to Sea-Level Rise, U.S. Atlantic Coast*; USGS: Reston, VA, USA, 1999; Volume 1, pp. 99–593.
22. Shaw, J.; Taylor, R.B.; Forbes, D.L.; Ruz, M.H. Sensitivity of the Canadian Coast to Sea-Level Rise. *Geol. Surv. Canada Bull.* **1998**, *505*, 114.
23. Rao, K.N.; Subraelu, P.; Rao, T.V.; Malini, B.H.; Ratheesh, R.; Bhattacharya, S.; Rajawat, A.S. Ajai Sea-Level Rise and Coastal Vulnerability: An Assessment of Andhra Pradesh Coast, India through Remote Sensing and GIS. *J. Coast. Conserv.* **2009**, *12*, 195–207. [CrossRef]
24. Karymbalis, E.; Chalkias, C.; Chalkias, G.; Grigoropoulou, E.; Manthos, G.; Ferentinou, M. Assessment of the Sensitivity of the Southern Coast of the Gulf of Corinth (Peloponnese, Greece) to Sea-Level Rise. *Cent. Eur. J. Geosci.* **2012**, *4*. [CrossRef]
25. EC, [European Commission] Living with Coastal Erosion in Europe—Sediment and Space for Sustainability. OPOCE, Luxembourg. 2004. Available online: http://www.eurosion.org/project/eurosion_en.pdf (accessed on 1 July 2016).

26. Mohanty, P.C.; Mahendra, R.S.; Nayak, R.K.; Kumar, T.S. Impact of Sea Level Rise and Coastal Slope on Shoreline Change along the Indian Coast. *Nat. Hazards* **2017**, *89*, 1227–1238. [CrossRef]
27. Pendleton, E.A.; Thieler, E.R.; Williams, S.J. *Coastal Vulnerability Assessment of Golden Gate National Recreation Area to Sea-Level Rise*; US Geological Survey: Woods Hole, MA, USA, 2005; pp. 1–23.
28. Pendleton, E.A.; Thieler, E.R.; Williams, S.J. Importance of Coastal Change Variables in Determining Vulnerability to Sea- and Lake-Level Change. *J. Coast. Res.* **2010**, *26*, 176–183. [CrossRef]
29. Alexandrakis, G.; Karditsa, A.; Poulos, S.E.; Ghionis, G.; Kampanis, N.A. Environmental Systems-Vol. III—An Assessment of the Vulnerability to Erosion of the Coastal Zone due to a Potential Rise of Sea Level: The Case of the Hellenic Aegean Coast. *Environ. Syst.* **2014**, *3*, 1–14.
30. Gaki-Papanastassiou, K.; Karymbalis, E.; Poulos, S.E.; Seni, A.; Zouva, C. Coastal Vulnerability Assessment to Sea-Level Rise Bαsed on Geomorphological and Oceanographical Parameters: The Case OfArgolikos Gulf, Peloponnese, Greece. *Hell. J. Geosci.* **2010**, *45*, 109–122.
31. Boumboulis, V.; Apostolopoulos, D.; Depountis, N.; Nikolakopoulos, K. The Importance of Geotechnical Evaluation and Shoreline Evolution in Coastal Vulnerability Index Calculations. *J. Mar. Sci. Eng.* **2021**, *9*, 423. [CrossRef]
32. Dimou, A.; Vassilakis, E.; Antoniou, V.E.N. An Assessment of the Coastal Erosion at Marathon East Attica (Greece). In Proceedings of the Panhellenic and International Geographical Conferences, Collection of Proceedings, Thessaloniki, Greece, 22–24 October 2015; pp. 1579–1587.
33. Faour, G.; Fayad, A.; Mhawej, M. GIS-Based Approach to the Assessment of Coastal Vulnerability to Sea Level Rise: Case Study on the Eastern Mediterranean. *J. Surv. Mapp. Eng.* **2013**, *1*, 41–48.
34. Flansburg, M.E.; Stockli, D.F.; Poulaki, E.M.; Soukis, K. Tectono-Magmatic and Stratigraphic Evolution of the Cycladic Basement, Ios Tectono - Magmatic and Stratigraphic Evolution of the Cycladic Basement, Ios Island, Greece. *Tectonics* **2019**, *38*, 2291–2316. [CrossRef]
35. Climatic Data for Selected Stations in Greece. Available online: http://www.emy.gr/emy/el/ (accessed on 8 October 2022).
36. Soukisian, T.; Hatzinaki, M.; Korres, G.; Papadopoulos, A.; Kallos, G.; Anadranistakis, E. *Wind and Wave Atlas of the Hellenic Seas*, 1st ed.; Hellenic Centre for Marine Research: Athens, Greece, 2007; ISBN 987 960 86651 9-4.
37. CORINE Land Cover. Available online: https://land.copernicus.eu/pan-european/corine-land-cover/clc2018. (accessed on 8 October 2022).
38. Thieler, E.R.; Himmelstoss, E.A.; Zichichi, J.L.; Ergul, A. *The Digital Shoreline Analysis System (DSAS) Version 4.0-an ArcGIS Extension for Calculating Shoreline Change (No. 2008-1278)*; US Geological Survey: Woods Hole, MA, USA, 2009.
39. Hellenic Navy Hydrographic Service. *Sea Level Statistics of Greek Ports*; Hellenic Navy Hydrographic Service: Athens, Greece, 2015.
40. Folk, R.L.; Ward, W.C. Brazos River Bar: A Study in the Significance of Grain Size Parameters. *J. Sediment. Petrol.* **1957**, *27*, 3–36. [CrossRef]